Deep brain stimulation of midbrain locomotor circuits in the freely moving pig

Stephano J. Chang[a,b,c], **Andrea J. Santamaria**[b], **Francisco J. Sanchez**[b], **Luz M. Villamil**[b], **Pedro Pinheiro Saraiva**[b], **Francisco Benavides**[b], **Yohjans Nunez-Gomez**[d], **Juan P. Solano**[d], **Ioan Opris**[b], **James D. Guest**[a,b,e], **Brian R. Noga**[a,b,e,*]

[a]Neuroscience Graduate Program, University of Miami Miller School of Medicine, Miami, FL, USA

[b]The Miami Project to Cure Paralysis, University of Miami Miller School of Medicine, Miami, FL, USA

[c]Division of Neurosurgery, Department of Surgery, University of British Columbia, Vancouver, BC, Canada

[d]Department of Pediatric Critical Care, University of Miami Miller School of Medicine, Miami, FL, USA

[e]Department of Neurological Surgery, University of Miami Miller School of Medicine, Miami, FL, USA

Abstract

Background: Deep brain stimulation (DBS) of the mesencephalic locomotor region (MLR) has been studied as a therapeutic target in rodent models of stroke, parkinsonism, and spinal cord injury. Clinical DBS trials have targeted the closely related pedunculopontine nucleus in patients with Parkinson's disease as a therapy for gait dysfunction, with mixed reported outcomes. Recent studies suggest that optimizing the MLR target could improve its effectiveness.

Objective: We sought to determine if stereotaxic targeting and DBS in the midbrain of the pig, in a region anatomically similar to that previously identified as the MLR in other species, could initiate and modulate ongoing locomotion, as a step towards generating a large animal neuromodulation model of gait.

*Corresponding author. The Miami Project to Cure Paralysis, University of Miami School of Medicine, 1095 NW 14th Terrace, Miami, FL, 33136, USA. bnoga@miami.edu (B.R. Noga).

Methods: We implanted Medtronic 3389 electrodes into putative MLR structures in Yucatan micropigs to characterize the locomotor effects of acute DBS in this region, using EMG recordings, joint kinematics, and speed measurements on a manual treadmill.

Results: MLR DBS initiated and augmented locomotion in freely moving micropigs. Effective locomotor sites centered around the cuneiform nucleus and stimulation frequency controlled locomotor speed and stepping frequency. Off-target stimulation evoked defensive and aversive behaviors that precluded locomotion in the animals.

Conclusion: Pigs appear to have an MLR and can be used to model neuromodulation of this gait-promoting center. These results indicate that the pig is a useful model to guide future clinical studies for optimizing MLR DBS in cases of gait deficiencies associated with such conditions as Parkinson's disease, spinal cord injury, or stroke.

Keywords

Deep brain stimulation; Mesencephalic locomotor region; Cuneiform nucleus; Pig; Locomotion; Defensive behavior

Introduction

Locomotion is essential for survival and allows an animal to navigate its environment for resources, mates, and shelter, or to detect and escape predators and other threats. It includes walking, running, swimming, flying, and slithering and is a complex and stereotypically repetitive motor behavior requiring the coordination of numerous muscle synergies and other bodily systems. The brainstem is thought to coordinate the control of many of these systems, including the integration and modulation of relevant sensory (and cognitive) inputs and the direct and indirect control of endocrine, cardiorespiratory, and musculoskeletal systems supporting locomotion [1]. The mesencephalic locomotor region (MLR) is an important control node identified in the midbrain of several species [2–5]. Electrophysiological and functional imaging evidence of a homologous structure in humans also exists [6,7], prompting interest in this region as a deep brain stimulation (DBS) target for gait disorders [8].

Recently, several MLR optogenetic studies have provided new insights into the circuit architecture of this region, distinguishing cell populations from the more dorsally located cuneiform nucleus (CnF) and the ventrally adjacent pedunculopontine nucleus (PPN) [9–11]. These studies found that photostimulation of glutamatergic CnF neurons robustly initiated locomotion with short latencies [9–11], while photostimulation of cholinergic PPN neurons could not [9,10]. Interestingly, these studies arrived at different interpretations on the contributions of glutamatergic PPN neurons, with two of the studies suggesting that photostimulation of this population fails to initiate locomotion [10,11]. A third study however, suggests that this population initiates a slower, exploratory type of locomotion [9]. These results have potential clinical importance, since DBS studies targeting this region over the past 15 years have exclusively targeted the PPN, with few efforts to optimize the target selection [12]. A pilot study of CnF-targeted DBS for gait freezing in Parkinson's disease patients is currently underway [13].

While optogenetics allow for cell-type-specific activation of neural circuits, technical challenges currently impede its clinical use. Thus, electrical mapping in higher animals provides important functional information that can be placed in the context of rodent optogenetics data. A detailed and systematic electrical characterization of the MLR in a large animal model is an important translational step with the following goals in mind: 1) to empirically identify optimal locations and stimulation parameters for electrical control of locomotor output in this region; and 2) to describe potential off-target effects, and develop strategies to minimize these side-effects [14]. The pig is increasingly recognized as a translational model in the neurosciences [15–19]. In particular, pigs have large, convoluted brains and spinal cords that are amenable to *in vivo* imaging with medical-grade MRI and CT scanners, and adult population-averaged brain templates have recently been developed for the Yucatan miniature breeds [20,21]. Furthermore, the pig brain is large enough to accommodate commercially available human DBS electrodes [15], making them a useful model for neuromodulation studies.

Materials and methods

Subjects

We tested 14 female Yucatan micropigs (*Sus scrofa domesticus*; age range 7 months–2 years; weight range at the time of testing: 22 kg–60 kg). All subjects were acquired from the same swine breeding facility (Sinclair BioResources, LLC), and housed either individually or in pairs in light-, noise-, and temperature-controlled pens. Only female animals were used as males obtain a size that becomes prohibitive to safe handling, and they were kept out of contact from males to minimize variations in estrous cycle. Animals were fed twice a day and given access to water ad libitum. All animal research activities were approved by our local Institutional Animal Care and Use Committee.

After the subjects were familiarized with the treadmill and open field testing, they were surgically implanted with internal EMG electrodes (Microprobes for Life Science, Gaithersburg, MD) to record flexor and extensor activity in the forelimbs and hindlimbs during locomotion. This was followed by surgical implantation of DBS electrodes (Medtronic 3389, Medtronic Inc., Minneapolis, MN), stereotaxically targeting the anatomical correlates (nuclei) of the MLR described for other species. After recovery from surgery (7–10 days), animals underwent gait assessment to ensure there were no gross deficits from DBS implantation, prior to assessment of the behavioral responses to DBS. In treadmill experiments (N = 10 animals), reflective ball markers were attached to key joints of the animal to record kinematics data. Furthermore, limb EMG activity, treadmill speed, and videos of the experiments were recorded, during the testing of the various DBS electrodes and stimulation parameters.

Surgical procedures

All surgical procedures were performed under sterile conditions and using a mixture of telazole (8 mg/kg) and xylazine (1.5 mg/kg) for anesthetic induction, and inhaled isoflurane (2%) for maintenance after endotracheal intubation. The subject's vitals were monitored using pulse oximetry, ECG and temperature probes, and non-invasive blood pressure cuffs.

EMG electrode implantation: A custom differential EMG device was constructed by Microprobes for Life Science using Cooner Teflon stranded stainless steel wires connected to a silicone encased Samtec 36 pin connector (Samtec Inc., New Albany, IN). Two wires were subcutaneously tunneled and implanted to each of the following muscles: *triceps brachii (lateral)*, *brachialis*, *tibialis anterior*, *lateral gastrocnemius*. The connector was externalized and secured through a small skin opening in the upper thoracic area. When not being used, the device was carefully wrapped in a protective covering placed over the dorsum of the animal. Periodic cleaning and maintenance of the device and the externalization point allowed for chronic EMG recordings for three months.

DBS implantation and brain imaging: A custom-built MRI compatible acrylic headframe was affixed to the pig skull at four points along the zygoma using aluminum screws, along with a palate bar. On the morning of surgery, a high-resolution T2-weighted MRI of the subject's brain was acquired in the headframe, with MRI fiducials for stereotaxic targeting. Data were acquired using a Siemens 3T Trio MRI scanner (Siemens, Erlangen, Germany) with Syngo MR Software (Numarus 4, VB-19). The imaging obtained was used to plan electrode trajectories targeting the putative MLR based on anatomical landmarks such as the inferior colliculus and the 4th ventricle. Over the course of the surgeries, we intentionally incorporated a small range into the target coordinates to sample different regions surrounding the putative MLR: on the P 6.0 mm coronal plane in the pig brain atlas [22], we targeted a region 5–7 mm lateral to the midline, and between 4 and 10 mm inferior to the origin in the supero-inferior axis. Trajectories were planned using the freely available "A Medical Imaging Data Examiner" (AMIDE, version 1.0.4) [23]. The subject was positioned prone on a custom-built platform with openings for the limbs to allow for intraoperative movements. Burr holes were drilled at the planned entry points, and a micromanipulator attached to the headframe was used to advance Medtronic 3389 DBS electrodes (Medtronic Inc., Minneapolis, MN) to the target. At the predicted target, we briefly switched the anesthesia to dexmedetomidine (0.2–1.5mcg/kg/h infusion) to allow for intraoperative stimulation and EMG recordings. DBS electrodes were fixed to the burr holes using dental cement and a plastic cap, and the proximal ends were tunneled subcutaneously out to the dorsum of the neck, where they were externalized and secured through a small opening in the skin. A post-operative CT scan was performed to confirm brain electrode positions. Subjects recovered for one week after implantation surgery prior to any DBS testing. When not being tested, the externalized electrodes were secured in a protective covering that was affixed to the dorsum of the neck.

Open field behavioral assessments

For electrode stimulation and EMG recordings, the animals were temporarily sedated with midazolam (0.4–2.0 mg/kg IM) and then reversed with flumazenil (0.02–0.04 mg/kg IM), allowing connection of the DBS and EMG electrodes to a Ripple Neuro Grapevine Scout system (Ripple LLC, Salt Lake City, UT). To prevent breakage of the connections, the animals were outfitted with a custom-made vest/harness to help protect the front ends and to facilitate animal handling. Electrical stimulation parameters evoking locomotion for the open field and treadmill tests ranged from: 20–1000 μA for current, 20–50Hz for frequency, and 200–1000μs for pulse width. Based on these stimulation parameters and

a conservative estimate of the current-distance constant of $K = 500$ μA/mm^2 reported in the literature, the upper limit of current spread would be approximately 1.5 mm, with the lower limit of current spread being 0.2 mm [24]. That stimulation using adjacent electrode contacts (edge to edge distance 0.5 mm apart) resulted in disappearance of locomotion suggests the effective spread was less than 0.5 mm. Subjects were placed into the open field, an enclosed area (approximately 3×4 m), with rubber mat flooring to prevent slippage during assessments. DBS and EMG recordings were conducted using the Trellis software (Ripple LLC, Salt Lake City, UT). A separate experimenter video recorded these sessions using a smartphone (30 frames/s, 1920×1080 resolution). Behaviors such as freezing, vocalizations, cowering, rotation, and locomotion occurring during stimulation were recorded.

Manual treadmill testing

Subjects' DBS and EMG electrodes were connected to the Ripple Neuro Scout system as described for the open field assessments. The subject was outfitted in a custom-made vest/harness and placed on our custom-built manual treadmill. This manual treadmill was constructed from an aluminum frame with plexiglass walls on either side, and a belt section constructed from an industrial roller conveyor outfitted with a treaded rubber belt. Large diameter (12 inches) rigid polyvinyl chloride tubes affixed to nylon wheels were placed at each end of the frame to allow for smooth transition and cycling of the treadmill. A magnet-based custom speedometer/odometer was constructed using a magnetic reed switch and an Arduino processor positioned on the treadmill frame adjacent to a wheel fitted with magnets. Based on the diameter of the wheel with magnets, Arduino code was written to calculate the speed of the treadmill given successive triggers of the reed switch by the magnets on the wheel.

Soft reflective ball markers were attached to key joints of the subject using Velcro attachments. A 6-camera Vicon MX motion capture system (Vicon, Oxford, UK) was used to record kinematics data, sampled at 120Hz using the Vicon Nexus 2.9 software. Thus, limb EMG activity, treadmill speed, kinematics data, and video recordings were collected from locomotion trials testing the various DBS electrodes and stimulation parameters.

Histology and immunohistochemistry

Under anesthesia, animals were perfused intracardially with a prefix solution containing 0.9% NaCl + Heparin and fixed with 4% paraformaldehyde in PBS, and brains and spinal cords were removed and post-fixed for 48h in 4% paraformaldehyde in PBS. The tissue was then rinsed in PBS and cryoprotected using gradients of sucrose for 3 days. Tissue was sectioned into 40-μm sagittal serial sections using a sliding microtome. Cholinergic neurons were visualized by incubating tissue sections for 24h with a goat anti-choline acetyltransferase (ChAT) primary antibody (AB144P, Millipore/Sigma) 1:500 in 0.1 M PBS containing 0.3% Triton X-100 and 5% Donkey Serum at 4 °C in gentle agitation. Sections were then incubated for 90 min using an Alexa Fluor 594 donkey anti-goat secondary antibody (A-11058, Thermo-Fisher Scientific) at 1:200. Control tissue sections were exposed to the secondary antibody only to discern actual labelling from autofluorescence. A series of sections were stained with Cresyl Violet staining to identify neuronal clusters.

Briefly, sections were mounted on glass slides, dried for 1h at room temperature, coated with Vectashield + DAPI (Vector Laboratories), then cover-slipped and stored in the dark at 4 °C. The sections were then scanned and captured using a VS120 Olympus Slide scanner equipped with a digital camera (Pike F–505C from Allied Vision). Examination of cells was performed using a Zeiss Axioline microscope and Stereo Investigator 5.0 (Microbrightfield Bioscience, Inc., Williston, VT, United States). Images were viewed using FIJI NIH software (Schneider et al., 2012).

Electrode localization

Electrodes were localized *in vivo* and blinded to behavioral outcomes, to ensure accurate and unbiased correlation of contact positions to behavioral effects. This was done using a post-operative CT scan (0.6 mm slices) in the Neuroimaging Informatics Technology Initiative (NifTI) format, which was rigidly registered to the pre-operative individual MRI using SPM12 (Wellcome Trust Center for Neuroimaging; https://www.fil.ion.ucl.ac.uk/spm/software/spm12/) [25]. These images were used to localize contact positions onto a population-averaged MRI brain template [20], by applying the transformations generated during the construction of this non-linear template to the corresponding rigidly registered CT images. Electrode localizations were performed using Lead-DBS software (https://www.lead-dbs.org/) [26], implemented in MATLAB 9.9 R2020b (The Mathworks Inc., Natick, MA). This method was confirmed in early animals (N = 3 animals) by comparing electrode track positions from histological sections. A separate 3D NifTI object estimating the position of the cholinergic cluster of neurons delineating the PPN was created based on ChAT immunohistochemistry in the pig brainstem (N = 3 animals) and superimposed with electrode positions for anatomical context.

Statistical analyses

For all tests, an α threshold of 0.05 was set to determine statistical significance. RStudio was used to perform statistical analyses. Data normality was tested with the Shapiro-Wilk test, and differences were interrogated with the Wilcoxon-rank sum test when comparing DBS OFF to DBS ON, or using one-way ANOVA when multiple DBS frequencies were tested in a single group of animals. A linear regression was performed to calculate a line of best fit for evaluating the relationship between stimulation frequency and locomotor speed as well as stepping frequency.

Results

Stereotaxic targeting and intraoperative stimulation of the MLR in the Yucatan micropig

Stereotaxic targeting of the MLR in our animals (N = 14 animals) was based on the Félix pig brain atlas [22], ChAT immunohistochemistry of the pig brainstem, and anatomical landmarks on pre-operative MRI for our subjects (Fig. 1). The CnF is depicted on a sagittal slice in the pig brain atlas at 4.6 mm lateral to the midline and was used as one of our putative targets for the MLR (Fig. 1A). Although the Félix pig brain atlas does not delineate a PPN nucleus, we designated our target for the PPN based on ChAT immunohistochemistry (Fig. 1B and C), which revealed a cluster of cholinergic neurons near the pontomesencephalic junction that has traditionally characterized the PPN [27,28].

Once we acquired an MRI of our animals (N = 14 animals) in the stereotaxic head frame, we estimated coordinates for our CnF and PPN targets using the cerebral aqueduct, the borders of the midbrain, and the midline as references. Trajectories were selected that were parallel to both the sagittal and coronal axes of the atlas (Fig. 1D and E), and electrode positions were confirmed using CT/MRI fusion (N = 14 animals; Fig. 1F). After advancing electrodes to our estimated targets, intraoperative stimulation (N = 14 animals) was applied unilaterally (left and right) to assess potential effects. Although the anesthetized animals did not exhibit actual locomotion, we were able to measure rhythmic and alternating movements in the limbs that could be detected through EMG recordings (N = 4 animals; Fig. 1G). These intraoperative EMG recordings demonstrated that EMG responses varied significantly even using adjacent contacts (edges 0.5 mm apart), suggesting that optimal targeting is important (Fig. 1G). Intraoperative stimulation of this region also appeared to evoke changes in heart rate (Fig. 1H) despite minimal gross limb movements, suggesting direct activation of brainstem cardiovascular centers [1,29–32].

Electrical stimulation of the MLR evokes locomotion in the freely moving pig

To characterize the MLR in the freely moving pig, we implanted DBS electrodes into putative MLR sites of subjects and used a custom-built manual treadmill that allowed the subjects to walk or run freely (Fig. 2A and B). DBS of putative MLR sites in 10 of 14 subjects initiated locomotion from rest, suggesting the existence of an MLR in pigs, as has been described in other vertebrates investigated to date [1–5,33–35] (Fig. 2C and D; Supplementary Video 1). EMG recordings during these stimulations confirmed that these responses were short-latency responses (Fig. 2E; mean latency to EMG burst = 759 ± 118 ms, n = 100 trials, N = 10 animals), and treadmill trials comparing MLR-evoked locomotion to spontaneous bouts of locomotion showed higher maximum speeds in the former (Fig. 2F; N = 6 animals, Wilcoxon rank-sum test, $p < 0.001$).

Supplementary video related to this article can be found at https://doi.org/10.1016/j.brs.2021.02.017

MLR stimulation frequency controls locomotor speed and stepping frequency

MLR stimulation augmented ongoing locomotion in all animals where it initiated locomotion. To increase our confidence that we had targeted the MLR, we tested if stimulation frequency could control locomotor speed or the frequency of locomotor movements – a hallmark of the MLR reported in prior studies in other species (Fig. 3) [3,5,33,36]. Simple linear regressions were calculated to predict stepping frequency and locomotor speed based on stimulation frequency (Fig. 3C and D). A significant regression equation was found to predict stepping frequency based on stimulation frequency ($F_{(1,34)}$ = 26.37, $p < 0.001$), with an R^2 of 0.707 (N = 3 animals, 3 trials per animal per stimulation frequency). Similarly, a significant regression equation was found to predict locomotor speed based on stimulation frequency ($F_{(1,34)}$ = 17.81, $p < 0.001$), with an R^2 of 0.624 (N = 3 animals, 3 trials per animal per stimulation frequency).

Effective sites for evoking locomotion cluster near the cuneiform nucleus and dorsal pedunculopontine nucleus

When the active contacts that were effective at evoking locomotion were plotted onto a population-averaged MRI brain template that was generated for the Yucatan micropig [20], we found that these contacts were grouped dorsal to the cluster of cholinergic neurons delineating the PPN, with the most ventral of these contacts reaching the most dorsal aspect of the cholinergic group of cells (Fig. 4A, D–F). Contacts that were positioned too medially presented with significant off-target effects that precluded effective locomotion, including freezing, cowering, and rotating behaviors (Fig. 4A–C).

Electrical stimulation nearby MLR sites evoke behaviors that may prevent locomotion

Electrode contacts in or along the border of the periaqueductal gray and in the superior colliculus commonly elicited defensive behaviors, ranging from freezing to defensive vocalizations and cowering (Fig. 5A). Loud and high-frequency vocalizations and posturing were frequently observed prior to retreat (Fig. 5B and C; Supplementary Video 2). Aversive responses such as freezing, cowering, and vocalizations stopped immediately with turning off stimulation (Fig. 5B). In two animals, we observed exploratory behavior, where the animal appeared to vigorously scan its environment (Supplementary Video 3).

Supplementary video related to this article can be found at https://doi.org/10.1016/j.brs.2021.02.017

Discussion

In this study, we stimulated putative MLR sites in the Yucatan micropig and characterized the effects on locomotion, as well as nearby off-target effects. Importantly, these off-target effects actively prevented effective locomotion, demonstrating the significance of electrode position. Within the MLR, DBS in intact pigs reliably initiates and strongly facilitates locomotion, suggesting that MLR DBS may evoke supraphysiological levels of locomotor activity [18]. We also found that effective stimulation sites cluster around the CnF and the dorsal PPN, consistent with prior literature in cats [1,3,37] and in rodents [38]. This observation also coincides with recent optogenetic studies in mice, which demonstrate that activation of glutamatergic neurons in the CnF has the strongest effect on initiating locomotion [9–11]. Notably, this may have clinical relevance given that most DBS studies in this region have targeted the slightly ventral PPN and may, at least in part, explain the mixed and less than satisfactory outcomes to date [8]. Our results suggest that targeting more dorsally, towards the CnF, may maximize the locomotor effects of MLR DBS, and this is supported by a recent PPN DBS study, which found that in Parkinson's disease patients with gait freezing, the best gait outcomes were associated with more dorsal active contact positions [39]. Finally, computer modeling studies of DBS in this region indicate that lead shifts of as little as 1 mm significantly decrease target activation selectivity, supporting that this degree of mistargeting is not trivial [40].

Mechanistically, glutamatergic neurons in the MLR activate reticulospinal and monoaminergic neurons in the medulla, which project to spinal locomotor networks to

promote gait [1,41]. Since the chronaxie of myelinated axons is typically orders of magnitude lower than that of cell bodies, DBS in the MLR likely exerts its effects mostly through axons entering, leaving, or passing through the region, rather than through the cells within the MLR directly [42]. Thus, while tracing studies and optogenetic dissection can identify the cells, and even components of cells, that are likely to evoke specific circuit functions, this information should be supplemented with electrical mapping to confirm the optimal electrode locations and stimulation parameters for DBS to elicit similar functional effects. Other important considerations include the diameter, membrane properties, and orientation of axons both in the circuit of interest as well as in functionally distinct nearby circuits. Through electrical mapping, we empirically determined the electrode positions, as well as the stimulation parameters, that optimally elicited locomotion while minimizing off-target effects.

Off-target effects

Our study revealed several off-target effects of stimulation in this region, most notably, a range of defensive behaviors that prevented locomotion. Freezing, defensive vocalizing, and asymmetric cowering were elicited, by DBS near the superior colliculus and the periaqueductal gray – two structures implicated in defensive behavior in animals [43–45]. In two animals, we observed exploratory behavior, evoked by low frequency (20Hz) stimulation of the lateral periaqueductal gray, which at higher frequencies (50Hz), elicited explosive galloping. While this seemed initially contradictory, it could make sense in the context of a risk perception spectrum – lower levels of risk perception may elicit behaviors such as exploration of an environment, or freezing, while higher levels of risk perception may elicit defensive vocalizations, cowering, and escape. Alternatively, current spread from this region to neighboring regions could explain both the exploratory locomotion (PPN) and galloping (CnF) observed. For instance, the exploratory behavior we recorded was strikingly similar to that evoked by optogenetic stimulation of PPN glutamatergic neurons in mice in the hole-board test [9].

Rotating behaviors were also observed, primarily with contacts positioned medially and ventral to the CnF. These were predominantly ipsiversive rotations that the subjects appeared to resist unsuccessfully, although, in some instances, contraversive rotations were also seen. Similar observations have been documented with electrical or chemical stimulation of this region in rodents, though there was no clear consensus on the underlying mechanism [46,47]. Based on the regional anatomy, the decussation of the tectospinal tract could potentially contribute to this turning behavior. Alternatively, with the recent demonstration that Chx10-expressing V2a reticulospinal neurons control ipsilaterally orienting movements and locomotion in mice, it may be that some of our observed turning behavior was the result of activating inputs to these specific reticulospinal neurons [48,49]. Finally, a few instances of grimacing (N = 2 animals) and ataxia (N = 2 animals) were evoked with stimulation ventral to the CnF. While based on a small number of data, these observations may have involved stimulation of the superior cerebellar peduncle (ataxia) and the medial or lateral lemniscus (grimacing). Stimulation of these regions would be cautioned in patients to avoid these potential side effects.

Conclusion

Acute DBS of the MLR in a freely moving pig model demonstrated robust initiation and significant augmentation of locomotion, with locomotor output controlled by stimulation frequency (20–50Hz). Electrode positions that were effective in initiating locomotion centered around the CnF and the dorsal part of the PPN, supporting previous basic science studies that have electrically mapped the best MLR sites in cats [1,3,36,37,50], as well as recent optogenetics and clinical studies on the region [9–11,39]. Off-target effects indicate the involvement of this region in fear and evasive activity. Recognizing that most stimulation is effected through activation of axon bundles, we think that 3-dimensional diffusion tensor mapping of regional anisotropy may inform the development of a detailed computational model of this region. Such maps may provide a useful *in silico* companion to our animal model, to more comprehensively query electrode positions and configurations optimally activating axonal elements of interest in the MLR, especially when considering newer and more complex directional electrodes. Our results support that targeting the CnF for DBS in Parkinson's Disease patients with freezing of gait may warrant investigation [13].

Supplementary Material

Refer to Web version on PubMed Central for supplementary material.

Acknowledgments

Abbreviations

MLR	Mesencephalic Locomotor Region
DBS	Deep brain stimulation
CnF	Cuneiform nucleus
PPN	Pedunculopontine nucleus
ChAT	choline acetyltransferase

References

[1]. Opris I, Dai X, Johnson DMG, Sanchez FJ, Villamil LM, Xie S, et al. Activation of brainstem neurons during mesencephalic locomotor region-evoked locomotion in the cat. Front Syst Neurosci 2019;13:69. [PubMed: 31798423]

[2]. Skinner RD, Garcia-Rill E. The mesencephalic locomotor region (MLR) in the rat. Brain Res 1984;323(2):385–9. [PubMed: 6525525]

[3]. Shik ML, Severin FV, Orlovskii GN. [Control of walking and running by means of electric stimulation of the midbrain]. Biofizika 1966;11(4):659–66. [PubMed: 6000625]

[4]. Eidelberg E, Walden JG, Nguyen LH. Locomotor control in macaque monkeys. Brain : J Neurol 1981;104(Pt 4):647–63.

[5]. Cabelguen JM, Bourcier-Lucas C, Dubuc R. Bimodal locomotion elicited by electrical stimulation of the midbrain in the salamander Notophthalmus viridescens. J Neurosci : The Off. J. Soc. Neurosci 2003;23(6):2434–9.

[6]. Jahn K, Deutschlander A, Stephan T, Kalla R, Wiesmann M, Strupp M, et al. Imaging human supraspinal locomotor centers in brainstem and cerebellum. Neuroimage 2008;39(2):786–92. [PubMed: 18029199]

[7]. Piallat B, Chabardes S, Torres N, Fraix V, Goetz L, Seigneuret E, et al. Gait is associated with an increase in tonic firing of the sub-cuneiform nucleus neurons. Neuroscience 2009;158(4):1201–5. [PubMed: 19063948]

[8]. Chang SJ, Cajigas I, Opris I, Guest JD, Noga BR. Dissecting brainstem locomotor circuits: converging evidence for cuneiform nucleus stimulation. Front Syst Neurosci 2020;14(64).

[9]. Caggiano V, Leiras R, Goni-Erro H, Masini D, Bellardita C, Bouvier J, et al. Midbrain circuits that set locomotor speed and gait selection. Nature 2018;553(7689):455–60. [PubMed: 29342142]

[10]. Josset N, Roussel M, Lemieux M, Lafrance-Zoubga D, Rastqar A, Bretzner F. Distinct contributions of mesencephalic locomotor region nuclei to locomotor control in the freely behaving mouse. Curr Biol : CB 2018;28(6):884–901. e3. [PubMed: 29526593]

[11]. Dautan D, Kovács A, Bayasgalan T, Diaz-Acevedo MA, Pal B, Mena-Segovia J. Modulation of motor behavior by the mesencephalic locomotor region. 2020. bioRxiv [Preprint] Available at: 10.1101/2020.06.25.172296. [Accessed 24 July 2020].

[12]. Thevathasan W, Debu B, Aziz T, Bloem BR, Blahak C, Butson C, et al. Pedunculopontine nucleus deep brain stimulation in Parkinson's disease: a clinical review. Mov Disord : Off. J. Move. Disorder Soc 2018;33(1):10–20.

[13]. Chang SJ, Cajigas I, Guest JD, Noga BR, Luca CC, Jagid JR. Deep brain stimulation of the cuneiform nucleus for levodopa-resistant freezing of gait in Parkinson's disease: study protocol for a prospective, pilot trial. Pilot and feasibility studies. 2020 [Preprint] Available at: 10.21203/rs.3.rs-60496/v1.

[14]. Depoortere R, Sandner G, Di Scala G. Aversion induced by electrical stimulation of the mesencephalic locomotor region in the intact and freely moving rat. Physiol Behav 1990;47(3):561–7. [PubMed: 2359770]

[15]. Sauleau P, Lapouble E, Val-Laillet D, Malbert CH. The pig model in brain imaging and neurosurgery. Animal : An Int. J. Animal Biosci 2009;3(8):1138–51.

[16]. Lee JH, Jones CF, Okon EB, Anderson L, Tigchelaar S, Kooner P, et al. A novel porcine model of traumatic thoracic spinal cord injury. J Neurotrauma 2013;30(3):142–59. [PubMed: 23316955]

[17]. Lind NM, Moustgaard A, Jelsing J, Vajta G, Cumming P, Hansen AK. The use of pigs in neuroscience: modeling brain disorders. Neurosci Biobehav Rev 2007;31(5):728–51. [PubMed: 17445892]

[18]. Noga BR, Santamaria AJ, Chang S, Benavides FD, Sanchez FJ, Villamil LM, et al. The micropig model of neurosurgery and spinal cord injury in experiments of motor control. In: Whelan PJ, Sharples S, editors. The neural control of movement: model systems and tools to study locomotor function. Academic Press/Elsevier; 2020.

[19]. Musk E An integrated brain-machine interface platform with thousands of channels. J Med Internet Res 2019;21(10):e16194. [PubMed: 31642810]

[20]. Chang SJ, Santamaria AJ, Sanchez FJ, Villamil LM, Pinheiro Saraiva P, Rodriguez J, et al. In vivo population averaged stereotaxic T2w MRI brain template for the adult yucatan micropig. Front Neuroanat 2020;14(89).

[21]. Norris C, Lisinski J, McNeil E, VanMeter JW, VandeVord P, LaConte SM. MRI brain templates of the male yucatan minipig. Available at: bioRxiv 2020.07.17.209064. 2020. 10.1101/2020.07.17.209064.

[22]. Félix B, Léger M-E, Albe-Fessard D, Marcilloux JC, Rampin O, Laplace JP, et al. Stereotaxic atlas of the pig brain. Brain Res Bull 1999;49(1):1–137. [PubMed: 10466025]

[23]. Loening AM, Gambhir SS. AMIDE: a free software tool for multimodality medical image analysis. Mol Imag 2003;2(3):131–7.

[24]. Tehovnik EJ. Electrical stimulation of neural tissue to evoke behavioral responses. J Neurosci Methods 1996;65(1):1–17. [PubMed: 8815302]

[25]. Ashburner J Computational anatomy with the SPM software. Magn Reson Imaging 2009;27(8):1163–74. [PubMed: 19249168]

[26]. Horn A, Kuhn AA. Lead-DBS: a toolbox for deep brain stimulation electrode localizations and visualizations. Neuroimage 2015;107:127–35. [PubMed: 25498389]

[27]. Martinez-Gonzalez C, Wang HL, Micklem BR, Bolam JP, Mena-Segovia J. Subpopulations of cholinergic, GABAergic and glutamatergic neurons in the pedunculopontine nucleus contain calcium-binding proteins and are heterogeneously distributed. Eur J Neurosci 2012;35(5):723–34. [PubMed: 22356461]

[28]. Mahady LJ, Perez SE, Emerich DF, Lu Wahlberg, Mufson EJ. Cholinergic profiles in the Goettingen miniature pig (Sus scrofa domesticus) brain. J Comp Neurol 2017;525(3):553–73. [PubMed: 27490949]

[29]. Korte SM, Jaarsma D, Luiten PG, Bohus B. Mesencephalic cuneiform nucleus and its ascending and descending projections serve stress-related cardiovascular responses in the rat. J Auton Nerv Syst 1992;41(1–2):157–76. [PubMed: 1491112]

[30]. Lam W, Gundlach AL, Verberne AJM. Increased nerve growth factor inducible-A gene and c-fos messenger RNA levels in the rat midbrain and hindbrain associated with the cardiovascular response to electrical stimulation of the mesencephalic cuneiform nucleus. Neuroscience 1996;71(1):193–211. [PubMed: 8834402]

[31]. Lam W, Gundlach AL, Verberne AJ. Neuronal activation in the forebrain following electrical stimulation of the cuneiform nucleus in the rat: hypothalamic expression of c-fos and NGFI-A messenger RNA. Neuroscience 1997;78(4):1069–85. [PubMed: 9174075]

[32]. Verberne AJ. Cuneiform nucleus stimulation produces activation of medullary sympathoexcitatory neurons in rats. Am J Physiol 1995;268(3 Pt 2):R752–8. [PubMed: 7900919]

[33]. Sirota MG, Di Prisco GV, Dubuc R. Stimulation of the mesencephalic locomotor region elicits controlled swimming in semi-intact lampreys. Eur J Neurosci 2000;12(11):4081–92. [PubMed: 11069605]

[34]. Bernau NA, Puzdrowski RL, Leonard RB. Identification of the midbrain locomotor region and its relation to descending locomotor pathways in the Atlantic stingray, Dasyatis sabina. Brain Res 1991;557(1–2):83–94. [PubMed: 1747771]

[35]. Marlinsky VV, Voitenko LP. The effect of procaine injection into the medullary reticular formation on forelimb muscle activity evoked by mesencephalic locomotor region and vestibular stimulation in the decerebrated Guinea-pig. Neuroscience 1991;45(3):753–9. [PubMed: 1775247]

[36]. Mori S, Sakamoto T, Ohta Y, Takakusaki K, Matsuyama K. Site-specific postural and locomotor changes evoked in awake, freely moving intact cats by stimulating the brainstem. Brain Res 1989;505(1):66–74. [PubMed: 2611678]

[37]. Takakusaki K, Chiba R, Nozu T, Okumura T. Brainstem control of locomotion and muscle tone with special reference to the role of the mesopontine tegmentum and medullary reticulospinal systems. J. Neural Transm (Vienna, Austria : 1996) 2016;123(7):695–729.

[38]. Noga BR, Sanchez FJ, Villamil LM, O'Toole C, Kasicki S, Olszewski M, et al. LFP oscillations in the mesencephalic locomotor region during voluntary locomotion. Front Neural Circ 2017;11:34.

[39]. Goetz L, Bhattacharjee M, Ferraye MU, Fraix V, Maineri C, Nosko D, et al. Deep brain stimulation of the pedunculopontine nucleus area in Parkinson disease: MRI-based anatomoclinical correlations and optimal target. Neurosurgery 2019;84(2):506–18. [PubMed: 29846707]

[40]. Zitella LM, Mohsenian K, Pahwa M, Gloeckner C, Johnson MD. Computational modeling of pedunculopontine nucleus deep brain stimulation. J Neural Eng 2013;10(4):045005. [PubMed: 23723145]

[41]. Capelli P, Pivetta C, Soledad Esposito M, Arber S. Locomotor speed control circuits in the caudal brainstem. Nature 2017;551(7680):373–7. [PubMed: 29059682]

[42]. Veerakumar A, Berton O. Cellular mechanisms of deep brain stimulation: activity-dependent focal circuit reprogramming? Current Opinion in behavioral sciences 2015;4:48–55. [PubMed: 26719852]

[43]. Isa K, Sooksawate T, Kobayashi K, Kobayashi K, Redgrave P, Isa T. Dissecting the tectal output channels for orienting and Defense responses. eNeuro 2020;7(5).

[44]. Lefler Y, Campagner D, Branco T. The role of the periaqueductal gray in escape behavior. Curr Opin Neurobiol 2020;60:115–21. [PubMed: 31864105]

[45]. Forcelli PA, Waguespack HF, Malkova L. Defensive vocalizations and motor asymmetry triggered by disinhibition of the periaqueductal gray in nonhuman primates. Front Neurosci 2017;11:163. [PubMed: 28424576]

[46]. Robinson TE. Electrical stimulation of the brain stem in freely moving rats: I. Effects on behavior. Physiol Behav 1978;21(2):223–31. [PubMed: 567820]

[47]. Sherman D, Fuller PM, Marcus J, Yu J, Zhang P, Chamberlin NL, et al. Anatomical location of the mesencephalic locomotor region and its possible role in locomotion, posture, cataplexy, and parkinsonism. Front Neurol 2015;6:140. [PubMed: 26157418]

[48]. Cregg JM, Leiras R, Montalant A, Wanken P, Wickersham IR, Kiehn O. Brainstem neurons that command mammalian locomotor asymmetries. Nat Neurosci 2020;23(6):730–40. [PubMed: 32393896]

[49]. Usseglio G, Gatier E, Heuzé A, Hérent C, Bouvier J. Control of orienting movements and locomotion by projection-defined subsets of brainstem V2a neurons. Curr Biol 2020;30(23):4665–81. e6. [PubMed: 33007251]

[50]. Sterman MB, Fairchild MD. Modification of locomotor performance by reticular formation and basal forebrain stimulation in the cat: evidence for reciprocal systems. Brain Res 1966;2(3):205–17. [PubMed: 6008190]

Significance statement

Recently, mouse optogenetics has provided new insight into the functional organization of midbrain locomotor circuits, pointing to glutamatergic neurons within the Cuneiform nucleus as an optimal locus for promoting gait. Clinically, this raised the question of whether the equivocal outcomes to date of deep brain stimulation (DBS) trials targeting the nearby Pedunculopontine nucleus for gait dysfunction were, at least in part, attributable to mistargeting. As part of a translational step towards answering this question, we provide detailed electrical characterization of midbrain sites controlling locomotion, as well as side-effects, in a freely moving large animal model: the swine. Our results demonstrate the utility of the pig as a large animal model for neuromodulation for gait.
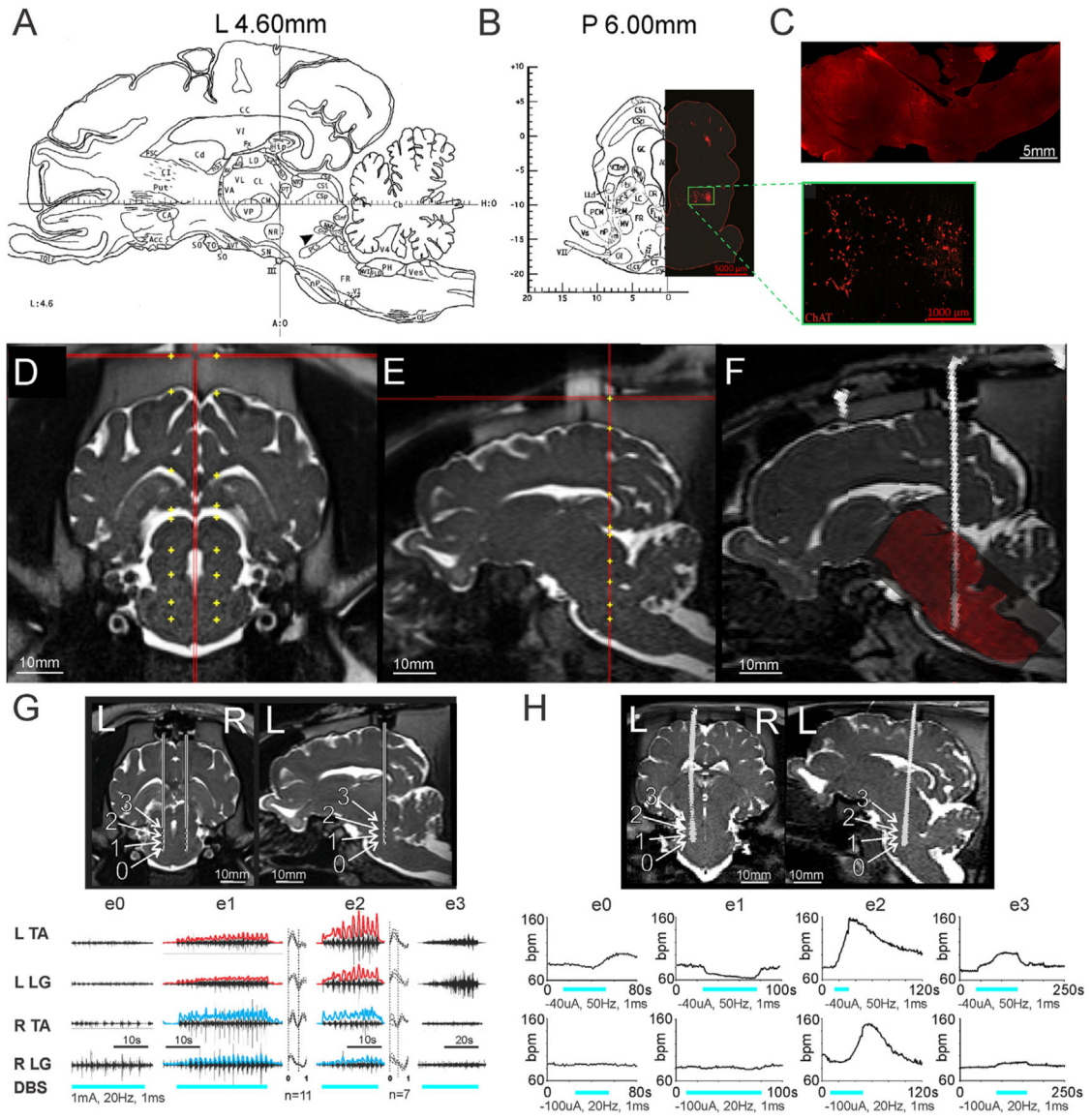
Fig. 1. Intraoperative stimulation of the MLR elicits locomotor-like EMG activity in the anesthetized pig.

(A) Sagittal slice from Félix et al. [22], at 4.6 mm lateral to midline depicts the location of the cuneiform nucleus (arrowhead, CnF), slightly inferior and anterior to the inferior colliculus. **(B)** *Left:* coronal slice from Félix et al. [22], at 6 mm posterior to the anterior limit of the posterior commissure at midline. *Right:* ChAT immunohistochemistry of a matched coronal slice, depicting a cluster of cholinergic neurons (green box, inset), traditionally defining the pedunculopontine nucleus, which is located ventral to the CnF. **(C)** ChAT immunohistochemistry of a sagittal brainstem slice similar to the atlas view in **(A)**, showing the cholinergic cluster ventral to electrode track. **(D)** Coronal and **(E)** sagittal views of example planned electrode trajectories targeting the MLR on pre-operative MRI. **(F)** Example of pre-op MRI/post-op CT fusion, with superimposition of post-mortem histology confirming electrode position via track. **(G)** *Top:* coronal view, bilateral electrode placement and sagittal section (left side) showing calculated positions of electrodes 0–3 (e0, e1, e2, e3).

Positions are approximations of the electrode size overlaid on the MRI cannula trajectory based on depth advanced. ***Bottom:*** EMG responses to stimulation of electrodes 0–3 on left side. Rectified and high pass filtered (>2Hz) traces of individual EMG traces from e1 and e2 are overlaid in red (left) and blue (right). Step cycle averages for e1 and e2 are shown on right of each muscle, with the number of step cycles averaged indicated. Repetitive EMG activity is observed with e1 and e2 stimulation, located within the cuneiform and adjacent subcuneiform region. EMG gain for each muscle is constant between trials. **(H)** ***Top:*** Coronal and sagittal views showing electrode position on CT scan superimposed onto brain MRI of another animal. ***Bottom:*** Heart rate responses to stimulation at each electrode position, using 20Hz or 50Hz stimulation. R: right, L: left, ECR: extensor carpi radialis; FCU: flexor carpi ulnaris; LG: lateral gastrocnemius, TA: tibialis anterior, SCL: step cycle length. For other atlas abbreviations please see Ref. [22]. G: From Noga et al. [18], with permission.
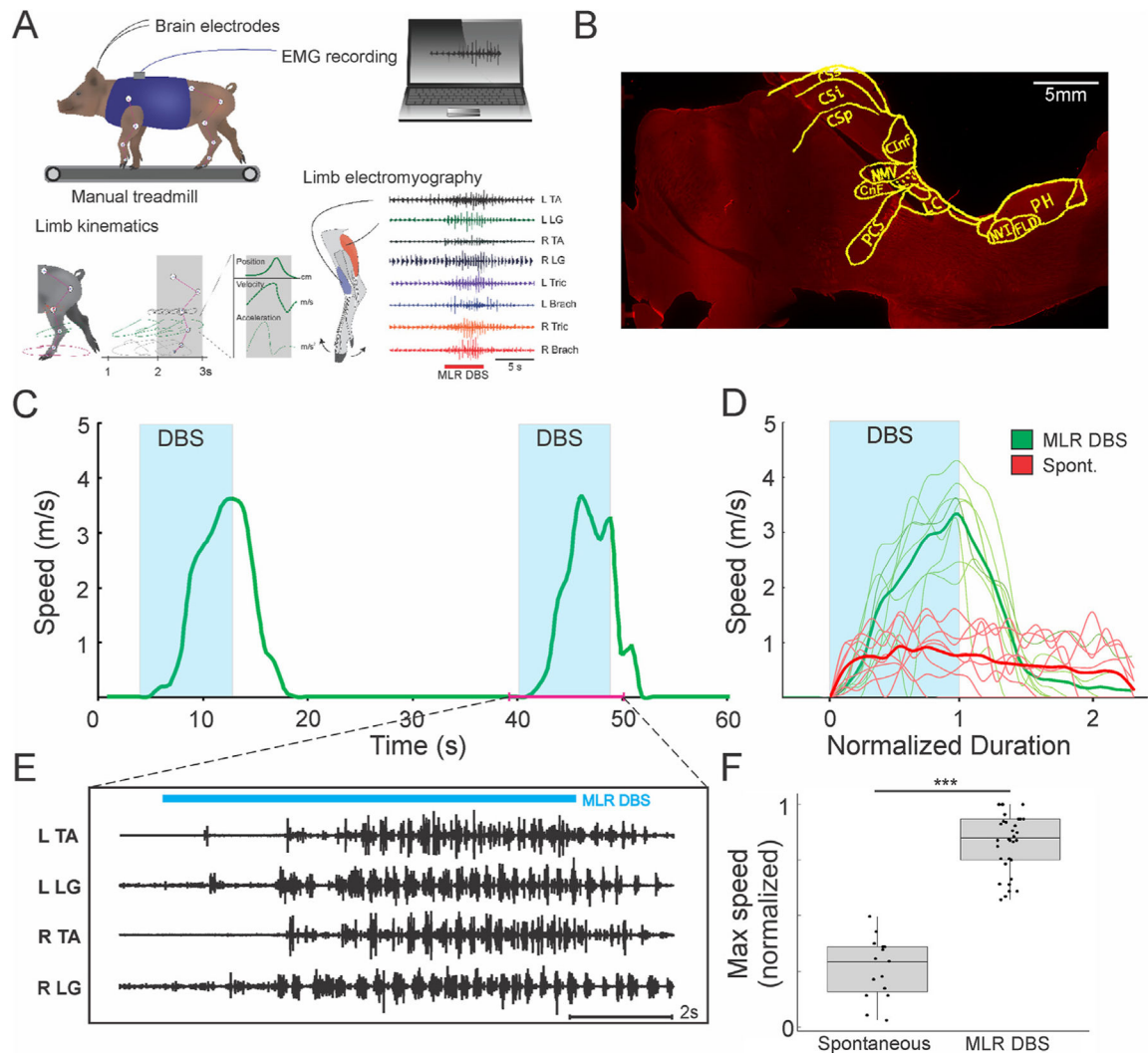
Fig. 2. Identification of MLR in the Yucatan micropig.
(**A**) Experimental setup for locomotor assessments in the freely moving pig. Subjects are connected to DBS and EMG electrodes and harnessed into a manual treadmill. Reflective ball markers are placed on major joints bilaterally, to simultaneously acquire speed, EMG, and kinematics data during locomotion. (**B**) Example of electrode track in a sagittal slice of the brainstem at 4.5 mm lateral to midline, with superimposition of anatomical features from the pig brain atlas [22]. CInf: inferior colliculus; CSi: intermediate layer of superior colliculus; CSp: deep layer of superior colliculus; CSs: superficial layer of superior colliculus; FLD: dorsal longitudinal fasciculus; LC: locus coeruleus; CnF: cuneiform nucleus; NMV: mesencephalic nucleus of trigeminal; NVI: nucleus of CN VI; PCS: superior cerebellar peduncle; PH: nucleus pre-positus hypoglossi. (**C, D**) Examples of MLR DBS initiating locomotion from rest (n = 8 trials MLR DBS, 7 trials spontaneous; left side unilateral stimulation, 0.1 mA, 20Hz, 1 ms pulse width, 8–12s duration) in one animal, with short latency to onset of EMG burst activity (**E**). For video see Supplementary Video 1. (**F**) MLR-evoked locomotion results in a higher maximum speed compared to spontaneous bouts of locomotion (n = 35 trials of MLR evoked locomotion, 14 trials of spontaneous

locomotion; N = 6 animals; Wilcoxon rank-sum test, *** denotes p < 0.001). A: Adapted from Noga et al. [18], with permission.
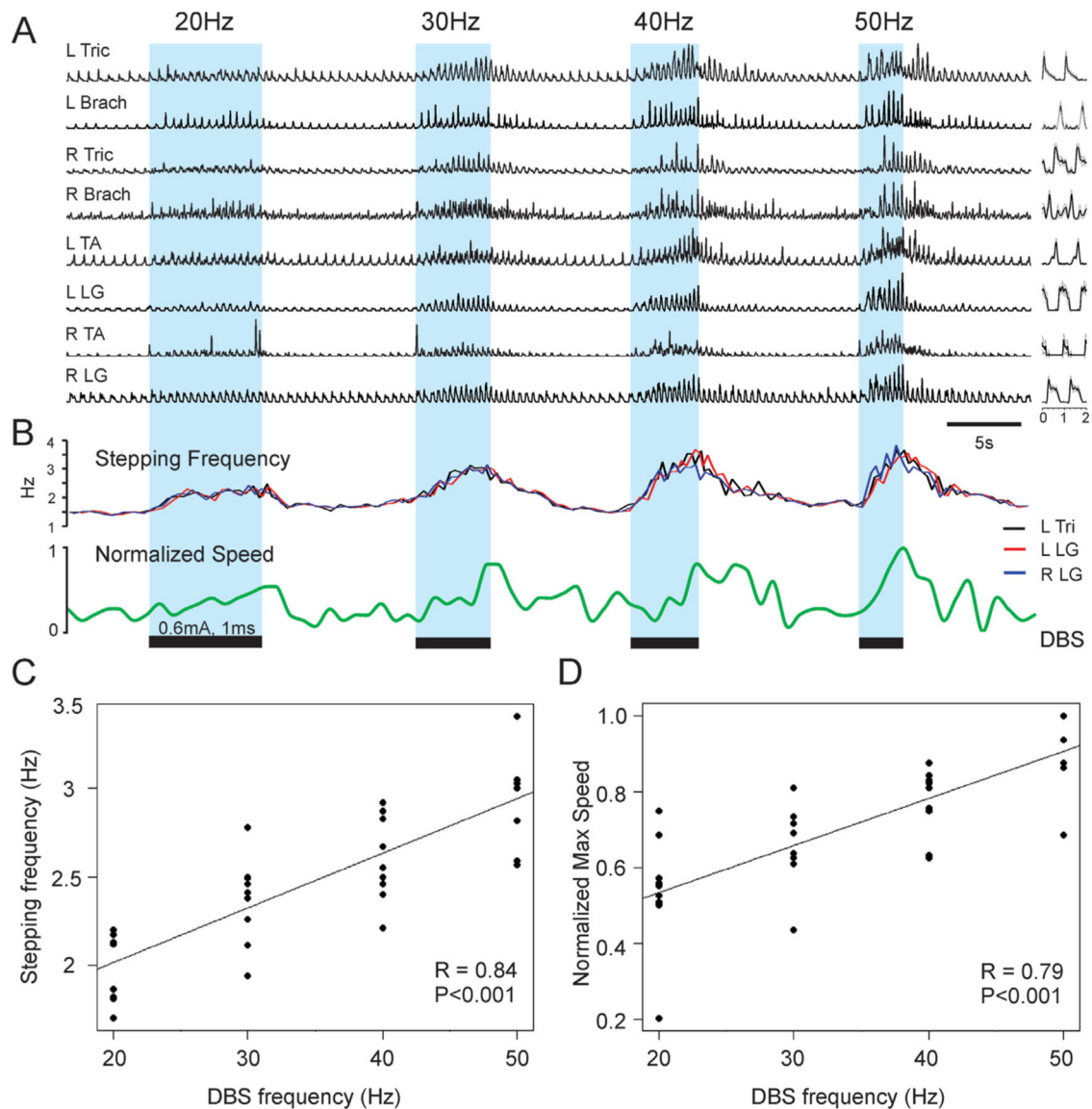
Fig. 3. MLR stimulation frequency controls locomotor output.
(A) Representative rectified and high pass filtered (>2Hz) EMG traces for extensors and flexors of each limb are shown during a treadmill trial, where MLR stimulation is applied at 20Hz, 30Hz, 40Hz, and 50Hz successively. **(B)** Traces showing stepping frequency and locomotor speed over time. **(C)** Relationship between stimulation frequency and stepping frequency. **(D)** Relationship between stimulation frequency and maximum locomotor speed. R: right, L: left, Tri: triceps, Brach: brachialis, TA: tibialis anterior, LG: lateral gastrocnemius, FL: forelimb, HL: hindlimb. A,B: modified with permission from Noga et al. [18].
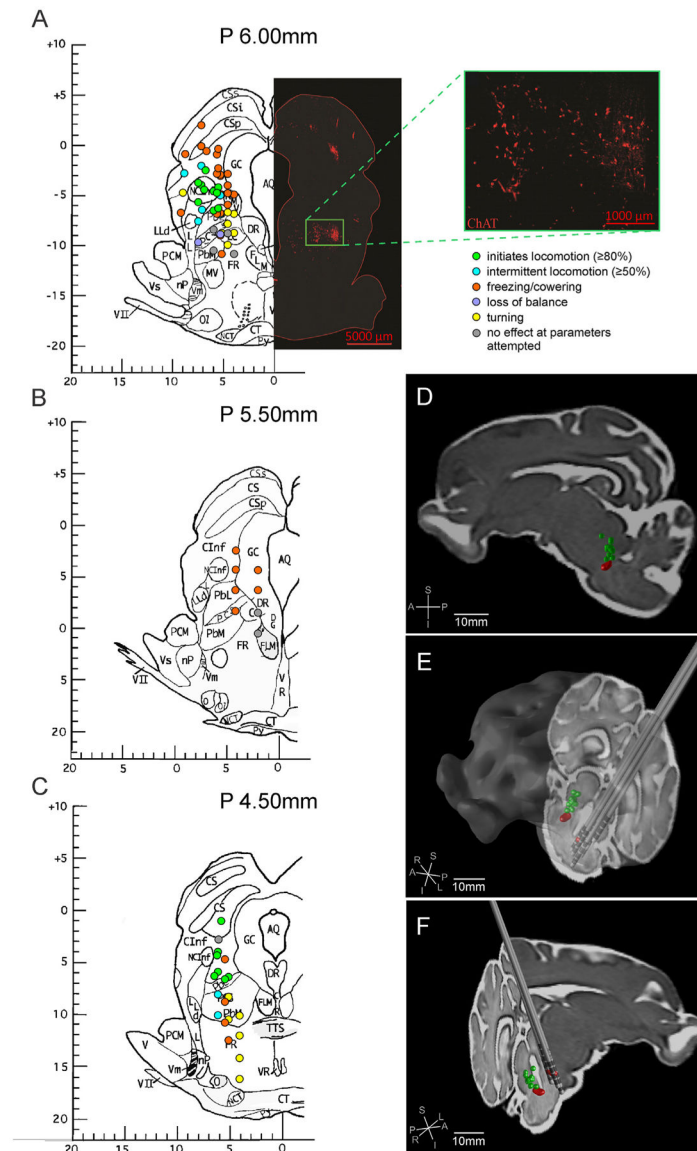
Fig. 4. Summary of stimulation sites and elicited behavioral effects.
Unilaterally stimulated electrode contact positions are overlaid on coronal slices at **(A)** 6 mm, **(B)** 5.5 mm, and **(C)** 4.5 mm posterior to the anterior limit of the posterior commissure on the Félix pig brain atlas [22]. The behaviors elicited with electrical stimulation were classified as shown in the legend in **(A)** and used to color code the electrode contact positions based on the behavior observed with stimulation. The ChAT immunohistochemistry of a matched coronal slice of the pig brainstem is included on the right side of the P 6 mm atlas slice to demonstrate the relative position of cholinergic neurons. **(D)** Parasagittal, **(E)** left oblique, and **(F)** right oblique three-dimensional views of effective electrode contacts for locomotion (green) are mirrored and plotted on the right side of the brainstem. The position of the cholinergic cluster of neurons representing the PPN are shown bilaterally (red) and the positions of implanted Medtronic 3389 electrodes are mirrored and plotted on the left side of the brainstem.
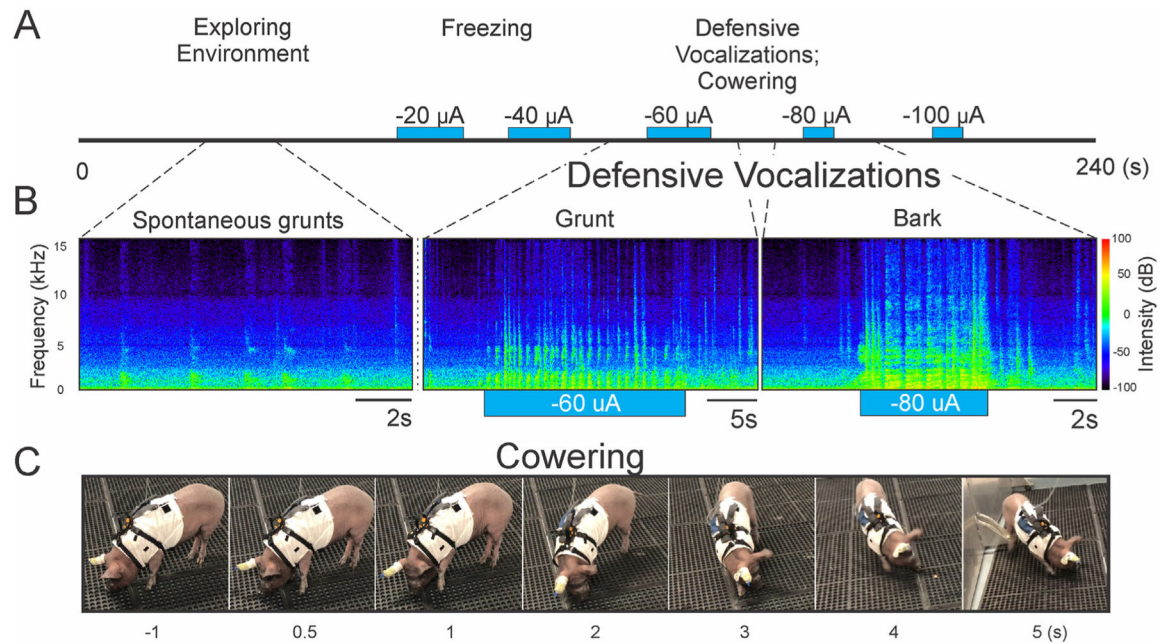
Fig. 5. Off-target stimulation results in defensive behaviors.
(A) Timeline for an example open field assessment trial is depicted, with off-target stimulation of increasing current. Behaviors ranged from freezing, to defensive vocalizations and cowering, as well as escape locomotion, depending on the intensity of stimulation. **(B)** Example audio spectrogram of spontaneous grunts, alongside defensive grunts and barks evoked with electrical stimulation. **(C)** Successive stills from a video depicting a typical evoked asymmetric cowering response in the open field. For full video see Supplementary Video 2.